

# CFD NUMERICAL SIMULATION OF BIODIESEL SYNTHESIS IN A SPINNING DISC REACTOR

Zhuqing Wen, Jerzy Petera \*

Politechnika Łódzka, Wydział Inżynierii Procesowej i Ochrony Środowiska, ul. Wólczańska 213,  
90-924 Łódź, Poland

In this paper a two-disc spinning disc reactor for intensified biodiesel synthesis is described and numerically simulated. The reactor consists of two flat discs, located coaxially and parallel to each other with a gap of 0.2 mm between the discs. The upper disc is located on a rotating shaft while the lower disc is stationary. The feed liquids, triglycerides (TG) and methanol are introduced coaxially along the centre line of rotating disc and stationary disc. Fluid hydrodynamics in the reactor for synthesis of biodiesel from TG and methanol in the presence of a sodium hydroxide catalyst are simulated, using convection-diffusion-reaction species transport model by the CFD software ANSYS©Fluent v. 13.0. The effect of the upper disc's spinning speed is evaluated. The results show that the rotational speed increase causes an increase of TG conversion despite the fact that the residence time decreases. Compared to data obtained from adequate experiments, the model shows a satisfactory agreement.

**Keywords:** spinning disc, biodiesel synthesis, ANSYS©Fluent, numerical simulation, TG conversion

## 1. INTRODUCTION

Biodiesel production involves the transesterification of oil or fat feedstock with methyl alcohol under alkaline conditions in a liquid-liquid environment. These include a wide range of vegetable oils such as sunflower oil, soya bean oil, peanut oil, and rapeseed oil. Another potential source of feedstock is waste tallow and fats derived from meat, fish and chicken processing facilities and from the rendering industry. There is also the potential to produce biodiesel from waste cooking oils, which are also a valuable feedstock for potential biodiesel production. Transesterification is a liquid-liquid two phase reaction at the interface between oils and alcohol because they are immiscible. In liquid-liquid reactions immiscible reactants must be transferred from one phase to another under diffusional regime before reaction takes place and this mass transfer can become the limiting step. Therefore, the efficiency of mass transfer is of importance for improving production capacity, reducing process cost and equipment size. It is desired that mass transfer rate is increased to a level allowing the reactions to proceed according to reaction kinetics (Krawczyk, 1996). Thus it is important to enhance contact and contact area between the two liquid phases and decrease resistance to mass transfer in the reactor. Conventional mechanical stirring or dispersion may improve the mass transfer but usually it is not satisfactory. The interfacial contact can be improved by establishing small-scale liquid structures or eddies within which mass transfer is enhanced (Green et al., 1999). Creating these small-scale liquid structures (micro mixing) is the role of new equipment and reactor design for coping with such immiscible systems .

\*Corresponding author, e-mail: jerzy.petera@p.lodz.pl

Spinning disc reactor (SDR) is one of the process intensification technologies employing high gravity fields caused by centrifugation. In some existing solutions of SDR, a high gravity field–centrifugal force is created by rotation of a disc surface on which liquid is dispersed as a thin film with the free surface of the liquid in contact with a gas. The gas may either be inert or contain a reactant, and may also act as a cooling or heating medium. When a liquid is introduced onto the disc surface at or adjacent to the spin axis, the liquid flows radially outward under the centrifugal force in the form of a thin film. At up to approximately 1000 rpm, these films are less than 100 microns thick and so offer a short diffusion path length (Stankiewicz and Moulijn, 2000). The film is unstable and forms waves at the gas-liquid interface. Unsteady film surface waves on the disc surface, coupled with the shearing action of the rotating surface, ensure that micro mixing and excellent mass and heat transfer are achieved (Jachuck, 2002). Extensive mass and heat transfer studies, and kinetic studies using this technology have shown that residence times, reactant inventories, and impurity levels can be reduced by up to 99% (Brechtelsbauer et al., 2001; Cafiero et al., 2002; Clifford et al., 2009).

A wide range of other applications of SDRs have been explored. Significant enhancements in polymerisation rates have been obtained within thin films generated on the rotating reaction surface, compared to classical stirred tank reactors. Continuous production of nano- and micro-size particles via reactive crystallisation in SDRs has also been reported (Dehkordi and Vafaeimanesh, 2009; Leveson et al., 2003; Meeuwse et al., 2010; Tai et al., 2006; Tai et al., 2007). Spinning disc reactors also have the potential for the intensification of both gas-liquid operations (Meeuwse et al., 2010) and liquid-liquid reactions (Dehkordi, 2002) due to their excellent mass transfer and uniform micro mixing characteristics. Extensive mass transfer studies using SDR have shown that mass transfer coefficient values in liquid-liquid system as high as  $30 \times 10^{-5} \text{ ms}^{-1}$  can be achieved due to the mentioned micro-mixing and an appropriate fluid dynamic environment for achieving faster reaction kinetics (Jachuck, 2002). Short residence time operation on the one hand may improve production efficiency and make continuous processes more viable. On the other hand, if the residence time is too short high conversion yields may not be achievable. In order to attain high effective reaction rates within a few seconds, mass transfer resistance must be reduced. Modified designs of spinning disc reactors which enhance liquid-liquid mass transfer and reaction rate have been described. For example one type involves two impinging jets which are introduced into rotating and stationary discs through two simple nozzles which are directed toward each other at the center of each disc (Lodhar and Jachuck, 2007). This type combines high mixing rate achievable through the impingement process combined with the high shear forces associated with the fluid in contact with the disc surfaces.

In the present research, a special version of SDR developed to explore the possibility of improving the efficiency of biodiesel production is described and used, as shown in Fig. 1. Although this SDR is well used in biodiesel production, it is still unclear how fluid hydrodynamics influenced its performance. In this situation the complex process can be investigated by numerical simulation using professional CFD software. ANSYS©Fluent 13.0 was chosen in the present research. Fluid hydrodynamics in the reactor for the synthesis of biodiesel were modelled using convection-diffusion-reaction multicomponent transport model. In particular the effect of upper disc's spinning speed was investigated. The results show that the rotational speed influences the residence time and triglyceride (TG) conversion exhibits the same tendency as data obtained from adequate experiments. A quantitative comparison is also given and discussed.

## 2. EXPERIMENTAL SETUP AND MECHANISM OF ALKALI-CATALYSED TRANSESTERIFICATION REACTION

The experimental setup was built and described by Zheyang Qiu and Weatherley (Qiu et al., 2012), who are our collaborative partners from Department of Chemical and Petroleum Engineering, Kansas University, USA. We used their experimental data to verify our simulation results. The SDR system

consisted of two parallel coaxial discs: one stationary and the other rotational with controllable rotational speed. The discs in the present research were separated by a gap equal to 0.2 mm. The two immiscible liquid phases were pumped axially at the centers of the stationary disc and the spinning disc, with the speed of  $0.007 \text{ ms}^{-1}$  and  $0.006 \text{ ms}^{-1}$ . The model reaction system chosen for the study was the methyl-esterification of canola oil in the presence of a sodium hydroxide catalyst to form biodiesel and glycerol. Before being pumped into the SDR, sodium methoxide was prepared by dissolving sodium hydroxide in methanol. The experimental setup is shown in Fig. 1:

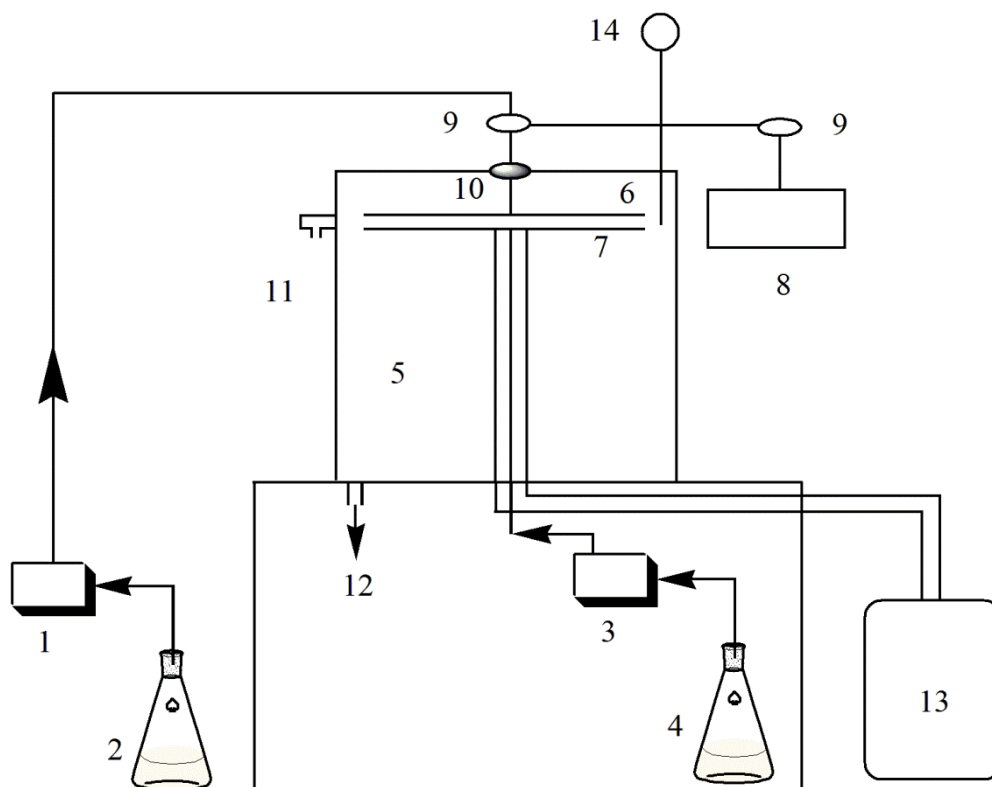


Fig. 1. Experimental setup of the intensive SDR for biodiesel synthesis;

- (1) peristaltic pump; (2) canola oil vessel; (3) digital piston pump; (4) sodium methoxide vessel; (5) cylinder; (6) rotating disc; (7) stationary disc; (8) variable-speed DC motor; (9) pulley; (10) bearing; (11) sampling point; (12) products drainage; (13) heating circulator; (14) thermometer

As mentioned above, biodiesel is mainly made by transesterification of vegetable oils and animal fats with alcohol in the presence of catalysts. Vegetable oils and animal fats typically consist of TGs which are esters of free fatty acids with the trihydric alcohol, glycerol.

For oil feedstock, rapeseed and soybean oils are most commonly used today, and canola oil was chosen in the present research. Also because of its low cost and high product efficiency, sodium hydroxide was chosen as the base catalyst. Basically, methanol is the cheapest alcohol available on the market, hence, it was chosen as the alcohol.

During the transesterification of TGs, there are three stepwise and reversible reactions with intermediate formation of diglycerides (DG) and monoglycerides (MG) resulting in the production of methyl esters ( $\text{RCOOCH}_3$ , biodiesel) and glycerol (GL) as shown in chemical equations I-III. The overall transesterification reaction is shown as chemical equation IV (Freedman et al., 1986; Nouredini and Zhu, 1997). The alcohol to TG molar ratio, catalyst type, reaction time and reaction temperature can affect the transesterification at different levels (Freedman et al., 1984).





In order to describe the chemical kinetics of the transesterification reaction, the following equations are used.

$$\begin{aligned} -r_I &= k_1 \cdot C_{TG} \cdot C_{CH_3OH} - k_2 \cdot C_{DG} \cdot C_{RCOOCH_3} \\ -r_{II} &= k_3 \cdot C_{DG} \cdot C_{CH_3OH} - k_4 \cdot C_{MG} \cdot C_{RCOOCH_3} \\ -r_{III} &= k_5 \cdot C_{MG} \cdot C_{CH_3OH} - k_6 \cdot C_{GL} \cdot C_{RCOOCH_3} \end{aligned} \quad (1)$$

where  $k_i$ ,  $i = 1, \dots, 6$  represent the respective kinetic constants that follow the Arrhenius equation:

$$k_i = A_i e^{-E_i/(RT)} \quad i = 1, 2, \dots, 6 \quad (2)$$

### 3. SIMULATIONS

ANSYS©Fluent v.13.0 was chosen to solve the chemical kinetics equations shown above. It is important to appropriately mesh the computational domain. To obtain a satisfactory mesh, it is necessary to simplify the real construction of SDR. As can be seen from Fig. 1, the region of interest is the space between the spinning and stationary discs. Since this construction is axisymmetric only half of the gap was simulated. Thus the computational domain is shown in Fig. 2.

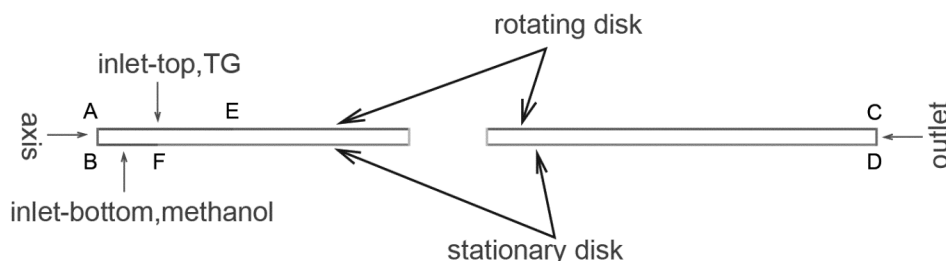


Fig. 2. Simplified computational domain of SDR

Dimensions of the domain based on the SDR construction are as follows. Domain radius AC: 50 mm; gap size AB: 0.2 mm; top inlet radius AE: 1.75 mm; bottom inlet radius BF: 0.77 mm. As mentioned before, TGs were pumped into the reactor through the orifice AE with the velocity of  $0.007 \text{ ms}^{-1}$  and methanol along orifice BF with the velocity  $0.006 \text{ ms}^{-1}$ , respectively. The corresponding volumetric flow rates of TG and methanol were  $5.77 \times 10^{-8} \text{ m}^3 \text{ s}^{-1}$  and  $1.3 \times 10^{-8} \text{ m}^3 \text{ s}^{-1}$ , respectively.

Two meshes were used in the present research. The information about the basic mesh is shown in Table 1 while the other, more refined mesh will be described later.

Table 1. The basic mesh information for the computational domain of SDR

Cells	Faces	Nodes
37515	77546	40032

### 3.1. Simulation methodology

Because the most important equations relevant to this simulation are species transport with reaction equations, all the flow (mass and momentum) equations are omitted in this description. ANSYS©Fluent predicts the local mass fractions of each species through the solution of convection-diffusion-reaction equation for each species. The general form of this equation is (ANSYS©Fluent v.13.0 Theory Guide, 2010):

$$\frac{\partial}{\partial t}(\rho Y_i) + \nabla \cdot (\rho v Y_i) = -\nabla \cdot J_i + R_i + S_i \quad (3)$$

An equation of this form will be solved for  $(n-1)$  species where  $n$  is the total number of chemical species present in the system. Since the mass fraction of the species must sum to unity, the  $n^{\text{th}}$  mass fraction is determined as one minus the sum of the  $(n-1)$  solved mass fractions. In the present research  $n = 6$ .

Reynolds number  $Re$  of reagents in the SDR in the present research was calculated using the following equation

$$Re = \frac{\rho N D d}{\mu} \quad (4)$$

Reynolds numbers for all six rotational speeds were calculated with the largest and smallest values equal to 211 and 105.5, respectively. This implied that the flow inside the spinning disc reactor was laminar. The physical properties were taken from available literature (Qiu, 2010).

Then, the diffusion flux of species  $i$ ,  $J_i$ ,  $i = 1, 2, \dots, 5$  which arises from the corresponding concentration gradients, were defined as

$$J_i = -\rho D_{i,m} \nabla Y_i \quad (5)$$

In the general equation (3) the symbol  $R_i$  is responsible for chemical reaction rates. For the calculation of chemical reactions, the laminar finite-rate model was used based on the Arrhenius expressions. The net source of chemical species  $i$  due to reaction  $R_i$  was computed as the sum of the Arrhenius reaction sources over the  $N_R$  reactions that the species participate in:

$$R_i = M_{w,i} \cdot \sum_{r=1}^{N_R} R'_{i,r} \quad (6)$$

In the present research, the species and reactions involved are shown in chemical equations I-III. The molar rate of creation/destruction of species  $i$  in reaction  $r$  ( $R'_{i,r}$  in Equation (6)) is given by

$$R'_{i,r} = (\vartheta''_{i,r} - \vartheta'_{i,r})(k_{f,r} \prod_{j=1}^{N_R} [C_{j,r}]^{\eta'_{j,r}} - k_{b,r} \prod_{j=1}^{N_R} [C_{j,r}]^{\eta''_{j,r}}) \quad (7)$$

According to chemical reaction equations in equations I-III, Equation (7) can be split into an explicit rate equation for each individual component (see Appendix).

The forward rate constant for reaction  $r$ ,  $k_{f,r}$ , is computed using the Arrhenius expression.

$$k_{f,r} = A_r e^{-E_r/RT} \quad (8)$$

In the present research, the kinetic rate constant and activation energy data were obtained and modified on the basis of data in Table 2.

For a reversible reaction the backward rate constant  $k_{b,r}$  for reaction  $r$  is determined by the following expression:

$$k_{b,r} = \frac{k_{f,r}}{K_r} \quad (9)$$

where  $K_r$  is the equilibrium constant for the reaction  $r$ , determined by the expression:

$$K_r = \exp\left(\frac{\Delta S_r^0}{R} - \frac{\Delta H_r^0}{R \cdot T}\right) \cdot \left(\frac{P_{atm}}{R \cdot T}\right)^{\sum_{i=1}^N (\vartheta''_{i,r} - \vartheta'_{i,r})} \quad (10)$$

$$\frac{\Delta S_r^0}{R} = \sum_{i=1}^N (\vartheta''_{i,r} - \vartheta'_{i,r}) \cdot \frac{S_i^0}{R} \quad (11)$$

$$\frac{\Delta H_r^0}{R \cdot T} = \sum_{i=1}^N (\vartheta''_{i,r} - \vartheta'_{i,r}) \cdot \frac{H_i^0}{R \cdot T} \quad (12)$$

Concerning the last term in the general equation (3),  $S_i$  equals zero because in the present research there is no additional source for species.

Table 2. Chemical kinetics data used and modified according to the units used in the software for all reactions (Noureddini and Zhu, 1997)

Parameter	Reaction I (TG → DG)	Reaction II (DG → MG)	Reaction III (MG → GL)
Kinetic rate constant, $k_i$	$8.333 \times 10^{-4}$	$3.583 \times 10^{-3}$	$4.033 \times 10^{-3}$
Activation energy, $E_i$	$5.5 \times 10^7$	$8.309 \times 10^7$	$2.687 \times 10^7$

### 3.2. Modelling assumptions and boundary conditions

For the purpose of modelling and in order to simplify the calculation, initial assumptions were made as follows:

- Feedstock from inlet-top and inlet-bottom was TG and methanol, respectively. Molar ratio of methanol to TG was 6:1, and concentration of NaOH was 1.0 wt%. Although there was no explicit occurrence of a catalyst, the presence of the catalyst was taken into account by modification of the rate constants in the kinetic equations;
- The problem was nearly isothermal because the thermal boundary conditions assumed perfect thermal control, thus all physicochemical properties were nearly constant. In the present research, all the cases were simulated under the temperature of 25°C.
- At the start the whole domain (the gap) was filled with TGs at rest and from this point the process started by injecting the substrates; TG and methanol.
- Reaction rates were determined by Arrhenius expressions, the effect of turbulent fluctuations was ignored.
- We assumed a single phase flow in the SDR due to the fact that mean droplet size was 257 nm at the rotational speed of 1000 rpm and the mean droplet size decreased with increase of the speed (Qiu, 2010). This indicated that droplet size in the SDR was small justifying the assumption. Nevertheless we did also two-phase flow simulation (multiphase-mixture model) for comparison purposes, which is more comprehensively discussed below.
- The order of magnitude for diffusion coefficients is  $10^{-9} \text{ m}^2\text{s}^{-1}$  (Cussler, 1997). On the basis of available diffusivity data (Egbuna et al., 2013) for natural oils, the diffusivity value for the reacting mixture was assumed constant and equal to  $7 \times 10^{-9} \text{ m}^2\text{s}^{-1}$  in the present research.
- The feedstock for inlet-top was canola oil (ConAgra Foods, USA) in experiments (Qiu, 2010). Generally the content of TG in canola oil is 94.4-99.1%, and the content of free fatty acids in canola oil is 0.4-1.2%, which can result in saponification reaction (Przybylski, 2007). Based on this information the experimental value of the content of TG in canola oil was assumed as 95%. Since in our numerical simulation pure TG was used as the feedstock, thus we recommend multiplying TG conversion obtained from simulation by the factor of 0.95 before comparing it (the simulation) with experimental results.

- Owing to the low level of free fatty acids content in canola oil and a relatively small amount of catalyst used in the experiment, combined with fast rotational speed of spinning disc which implied short residence time, saponification side reaction was ignored in the present research.

Available experimental data dictated the following modelling conditions:

- Due to the fact that canola oil, as a mixture of fatty acids, consists mainly of oleic acid, triolein ( $C_{57}H_{104}O_6$ ) was chosen as a representation of TG, then diolein ( $C_{39}H_{72}O_5$ ) as a representation of DG, monoolein ( $C_{21}H_{40}O_4$ ) as a representation of MG, and methyl oleate ( $C_{19}H_{36}O_2$ ) as a representation of the resulting methyl ester (biodiesel).
- The inlet velocities for TG (inlet-top) and methanol (inlet-bottom) were  $0.006 \text{ ms}^{-1}$  and  $0.007 \text{ ms}^{-1}$ , respectively;
- The temperature was  $25^\circ\text{C}$  everywhere.

In the present research six cases were calculated and analysed by varying the rotational speeds of the spinning disc. The overall boundary conditions for each case and the rotational speed of the spinning disc for each case are shown in Tables 3 and 4.

Table 3. Boundary conditions for each case

	AB	AE	BF	EC	FD	CD
Boundary type	Axis	Velocity-inlet	Velocity-inlet	Wall	Wall	Outflow
Temperature, K	-	298.15	298.15	298.15	298.15	-
Velocity, $\text{ms}^{-1}$	-	0.006	0.007	-	-	-
Rotational speed of spinning disc, rpm	-	-	-	1000 - 2000	-	-

Table 4. Rotational speed of spinning disc for each case

	case 1	case 2	case 3	case 4	case 5	case 6
Rotational speed of spinning disc, rpm	1000	1200	1400	1600	1800	2000

## 4. SIMULATION RESULTS

### 4.1. Hydrodynamics of reactants in SDR

Fig. 3 below shows velocity contours inside the SDR gap for the case 4. The vertical position of the picture is justified by the ANSYS©Fluent technicality. When the axisymmetric geometry is modelled, the direction of the swirl axis is assumed to be the X axis and the computational domain is situated above the X axis, as shown in the following figures.

Fig. 3 indicates that magnitude of the bulk circumferential velocity increases from bottom right to top left. Because of fast rotation, reacting mixture close to the spinning disc flows faster, and reaches the highest speed at the upper end of the reactor.

Fig. 4 shows the velocity vectors of inlet-top and inlet-bottom and interprets the impinging phenomenon in SDR clearly. TG and methanol were injected into SDR gap in the normal direction to boundaries, with the velocity of  $0.0006 \text{ ms}^{-1}$  and  $0.0007 \text{ ms}^{-1}$ , respectively. The axial velocity of two

liquids helped them mix and the mixture flowed towards outlet under the forces of centrifugal gravity afterwards.

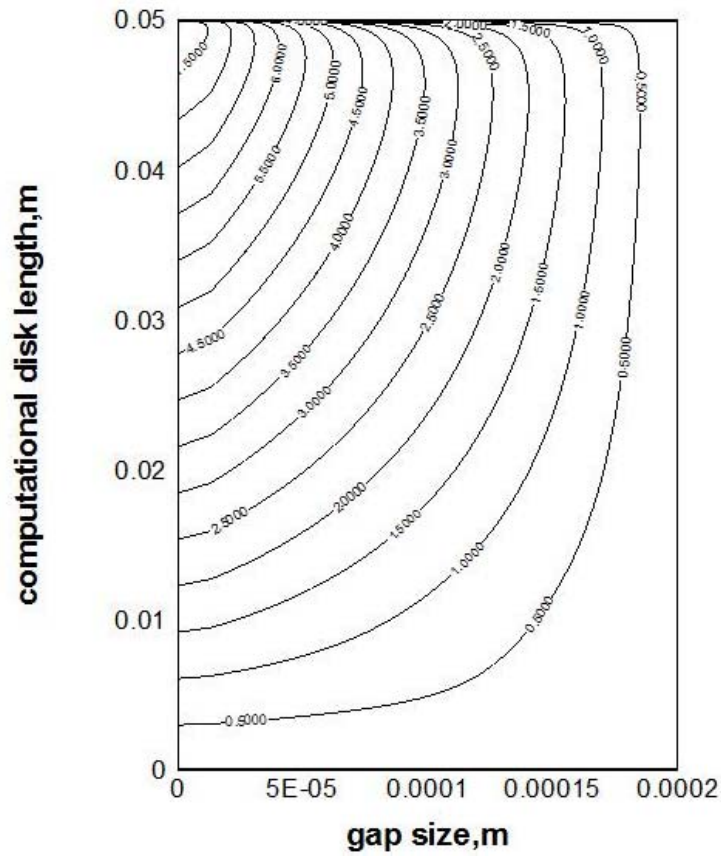


Fig. 3. Contours of inter-disc circumferential velocity in  $\text{ms}^{-1}$  (The geometry proportions are intentionally changed.)

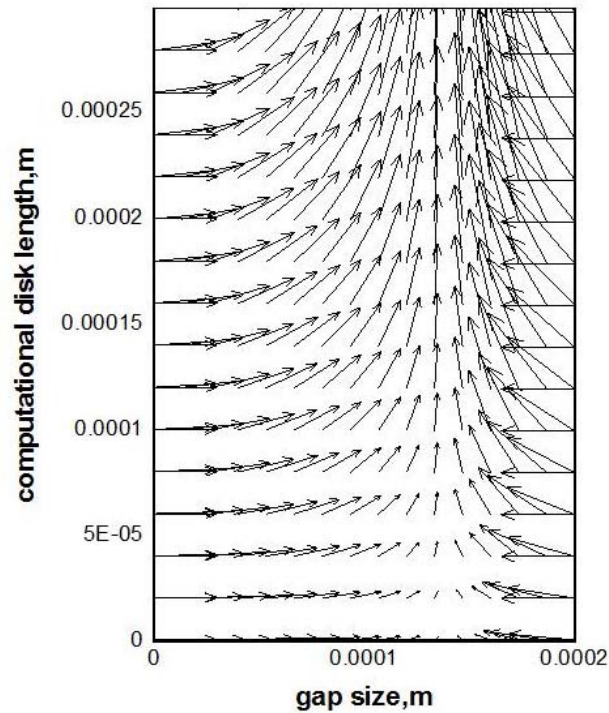


Fig. 4. Vectors of inlet-top and inlet-bottom in SDR (The geometry proportions are intentionally changed.)

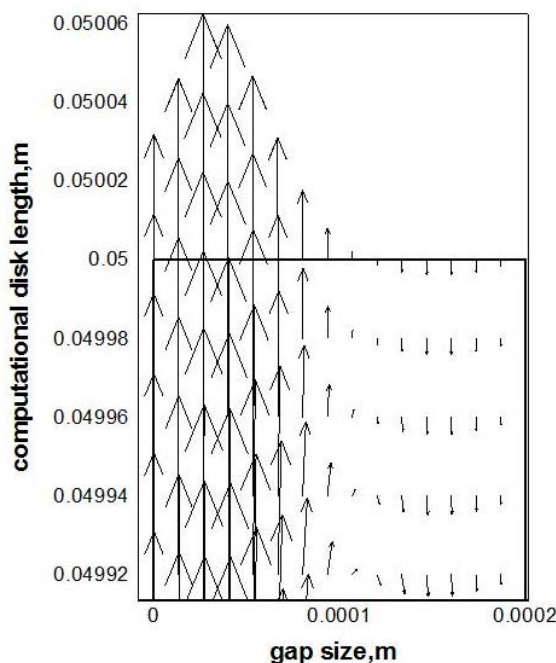


Fig. 5. Vectors at the outlet (The geometry proportions are intentionally changed.)

Fig. 5 presents velocity vectors at the outlet region. The flow profiles show the development of a reverse flow in the lower part of the gap and of the bulk liquid velocity profile from the outer extremity of the inter-disc gap towards the central region where the liquid mixes with the stream generated by the inlets. This can be explained as the influence of centrifugal force caused by the spinning disc rotation together with the continuity conservation, which in turn prevents liquid breakage. The development of a reverse flow is consistent with experimental observations in spinning disc reactors (Meeuwse et al., 2011). The velocity profile near the outlet is also consistent with published numerical results (Visscher et al., 2013). Such a phenomenon creates congenial conditions for controlling the residence time closely related to the reaction kinetics and the TG conversion as described below. There exists a class of solutions of the Navier-Stokes equations for steady rotationally-symmetric flow disc in literature (Childs, 2011; van Eeten et al., 2012). However, neither of them corresponds to the same boundary conditions as considered here.

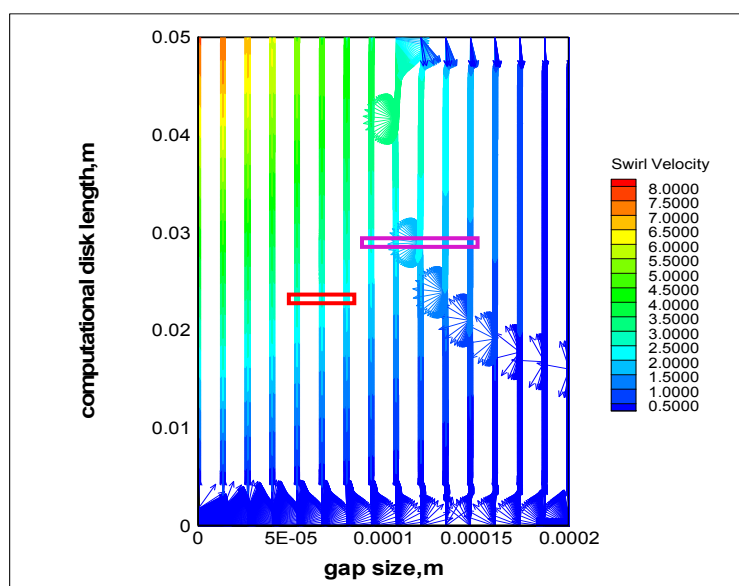


Fig. 6. Overall reverse flow zone within SDR gap in form of velocity vectors (The geometry proportions are intentionally changed)

Fig. 6 presents the reverse flow zone inside the inter-disc space showing a characteristic pattern, while Fig. 7 and Fig. 8 represent magnification of that secondary flow including an interesting impinging phenomenon, respectively. A pattern such as the one shown in Fig. 8 indicates where the reverse flow meets with the predominant outward stream, and flow together outwards outlet after meeting. The boarder of this zone may move with spinning rate increase.

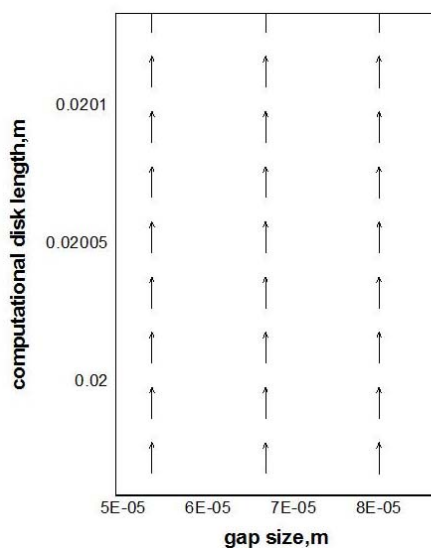


Fig. 7. Magnification of the outward flow marked in red frame in Fig. 6  
(The geometry proportions are intentionally changed)

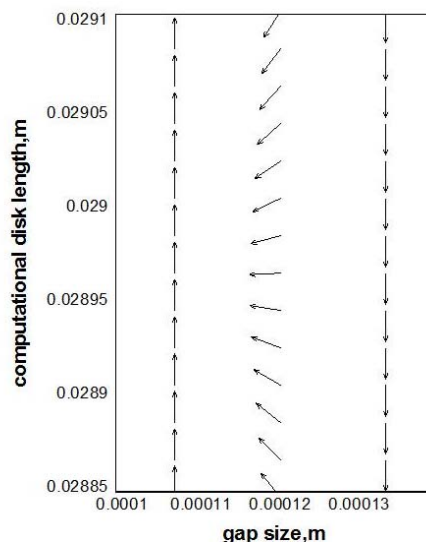


Fig. 8. Magnification of the impinging phenomenon marked in purple frame in Fig. 6  
(The geometry proportions are intentionally changed)

Fig. 9 shows the normalised molar concentration of methanol at the outlet as a function of time, which is the response to the step change of the methanol concentration at the inlet. Molar concentration of methanol at the outlet thus represents the cumulative probability function, and reaches a steady value when reactions reach the equilibrium state. The normalisation was done by dividing the maximum limit value of the concentration. The normalised curves were used for evaluation of the residence time for each rotational speed. The time when the rate of increase of a normalised molar concentration of methanol at the outlet reached the largest value was taken as the residence time at the corresponding rotational speed.

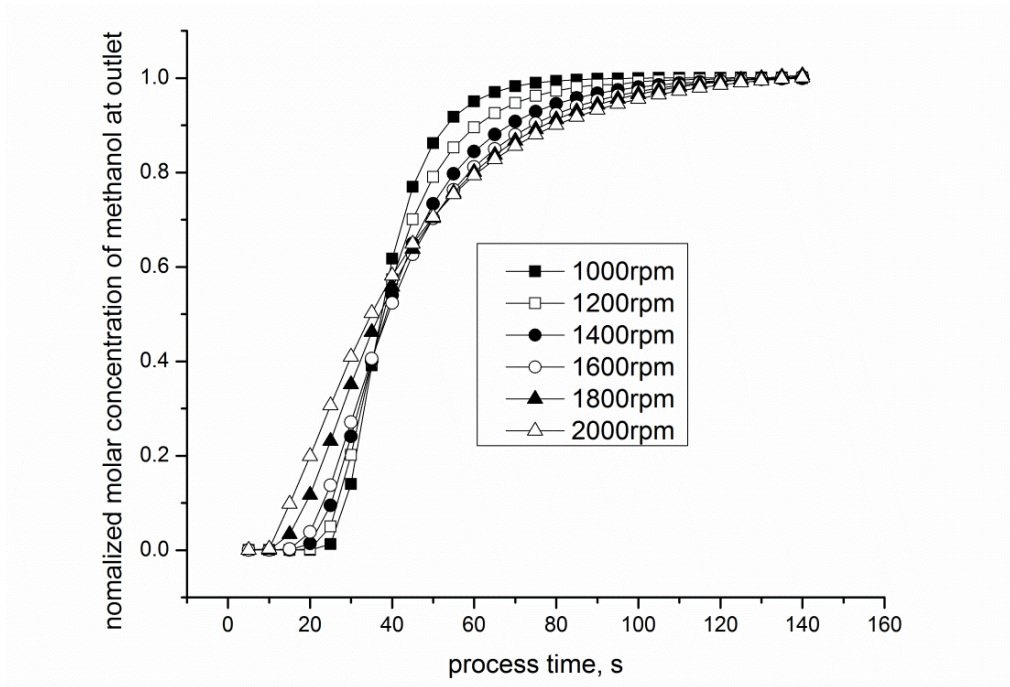


Fig. 9. Normalised molar concentration of methanol at the outlet during process time.

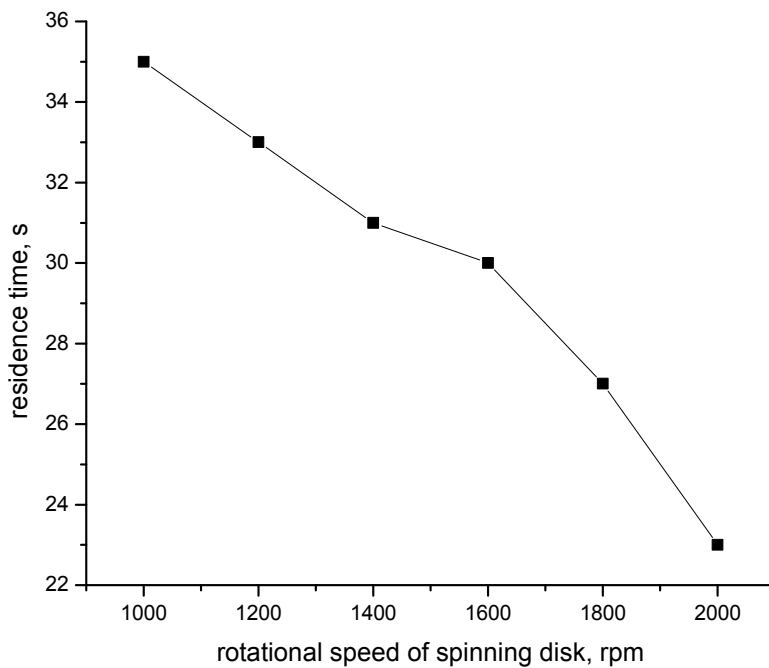


Fig. 10. Residence time of feedstock vs. the rotational speed of spinning disc

Figure 10 shows the residence time as the function of the spinning disc rotational speed. As can be seen, the residence time decreases from around 35 s when the rotational speed equals 1000 rpm to a value of around 23 s at the rotational speed of 2000 rpm.

As mentioned before, short residence time operation is desired for production efficiency but on the other hand a too short residence time may be not sufficient for the reaction to achieve high conversion.

#### 4.2. TG conversion attained by simulation

TG conversion is an adequate parameter to verify the accuracy of ANSYS©Fluent numerical simulation. To determine values of TG conversion  $\kappa$ , the following equation was used:

$$\kappa = \frac{C_0 \cdot Q_{v0} - C_k \cdot Q_{vk}}{C_0 \cdot Q_{v0}} \cdot 100\% \quad (13)$$

All the above variables,  $C_0$ ,  $C_k$ ,  $Q_{v0}$ ,  $Q_{vk}$ , can be read directly from ANSYS©Fluent Reports.

NaOH concentration highly influences kinetics, especially the pre-exponential factor in Arrhenius equation. Although the concentration of NaOH used is 0.2 wt% in Nouredini and Zhu's work, it is 1.0 wt% in the present paper. In order to evaluate the kinetic rate constants adequately for the present catalyst concentration we designed a method of optimal fitting of simulated conversion results (based on modified kinetic constants) to the experimental results described as follows. Five sets of kinetic constant data were used in the present research, namely 12 { $k_0$ }, 12.5 { $k_0$ }, 13 { $k_0$ }, 13.5 { $k_0$ } and 14 { $k_0$ }, where { $k_0$ } represents kinetic constant data used by Nouredini and Zhu (obtained for 0.2% catalyst content). All TG conversions for the six cases obtained from simulation are compared with the experiment in Fig. 11.

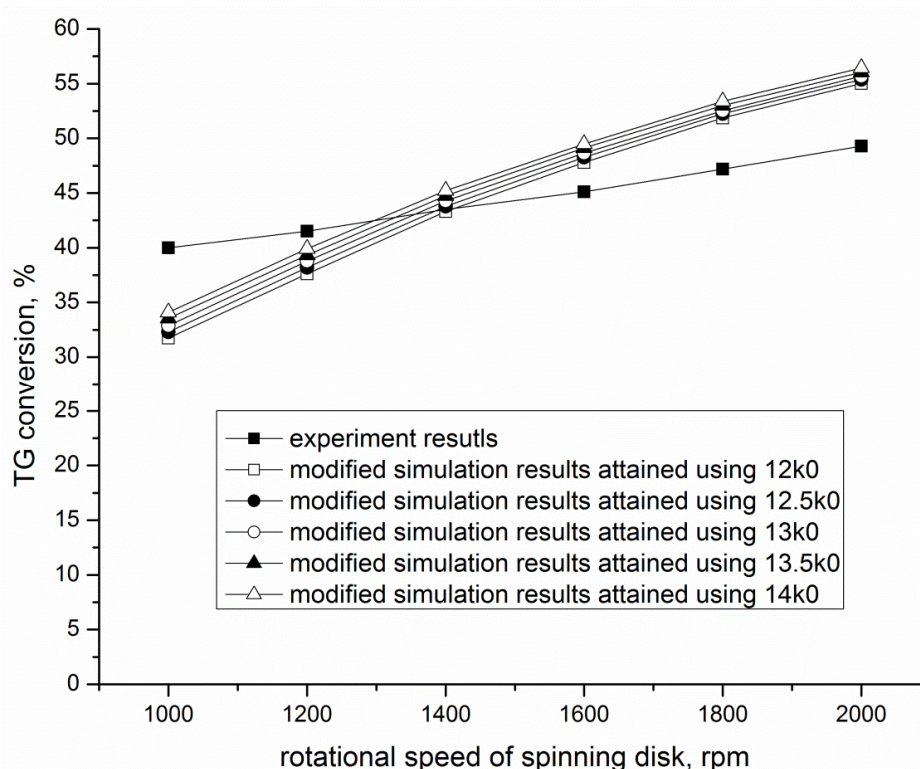


Fig. 11. TG conversions attained by simulation compared with those attained by experiment

Undoubtedly we can observe qualitative agreement between modified simulation results and experimental data, as TG conversion increases with the growing rotational speed of spinning disc. This can be explained by the fact that fast rotational speed enhances mixing among reagents by generating high shear forces, then eliminates transport resistance and thus improves TG conversion. Moreover as Fig.10 shows, the residence time decreases as the rotational speed of spinning disc increases, short residence time leads to less saponification and emulsification, this also helps improve TG conversion. Besides, probably a faster rotational speed of the spinning disc results in expanding reverse flow zone in the SDR, which helps reactants react more completely.

On the basis of the mean square root error calculation we concluded that  $13\{k_0\}$ , variant represents the best fitting to the experimental data, and we postulate using such evaluated kinetic rate constants as adequate for the present catalyst content. This is in agreement with conclusion from a previous paper (Qiu et al., 2012) where such multiplication was also recommended despite the fact that completely different software was used there. Experimental results by Nouredini and Zhu (Nouredini and Zhu, 1997) were probably obtained outside the strictly kinetical regime.

To verify mesh dependent accuracy we repeated the simulation using a more refined mesh described in Table 5. The results (not shown here) proved that there were no differences between results obtained from both meshes.

Table 5. Refined mesh information for the computational domain of SDR

Cells	Faces	Nodes
100035	205088	105054

In the present research, single phase flow was assumed due to the fast rotational speed of the spinning disc and efficient mixing of liquids. To verify the reliability of single phase flow model, a multiphase-mixture model (available as an option in ANSYS©Fluent software) was also simulated for comparison purposes. Owing to fast rotational speed of the spinning disc, TG and methanol contacted through the interphase in the SDR and the whole computational domain was filled with reaction mixture. Considering that the volumetric flow rate ratio of TG at inlet-top to methanol at inlet-bottom was 4.4, TG was set as the primary phase, and methanol was set as the secondary phase in the multiphase-mixture model. Besides, considering a rather small mean droplet size at the spinning disc rotational speed of 1000 rpm, droplet size was set as 257 nm for each case, and mass transfer coefficient was set as  $30 \times 10^{-5} \text{ ms}^{-1}$  for each case.

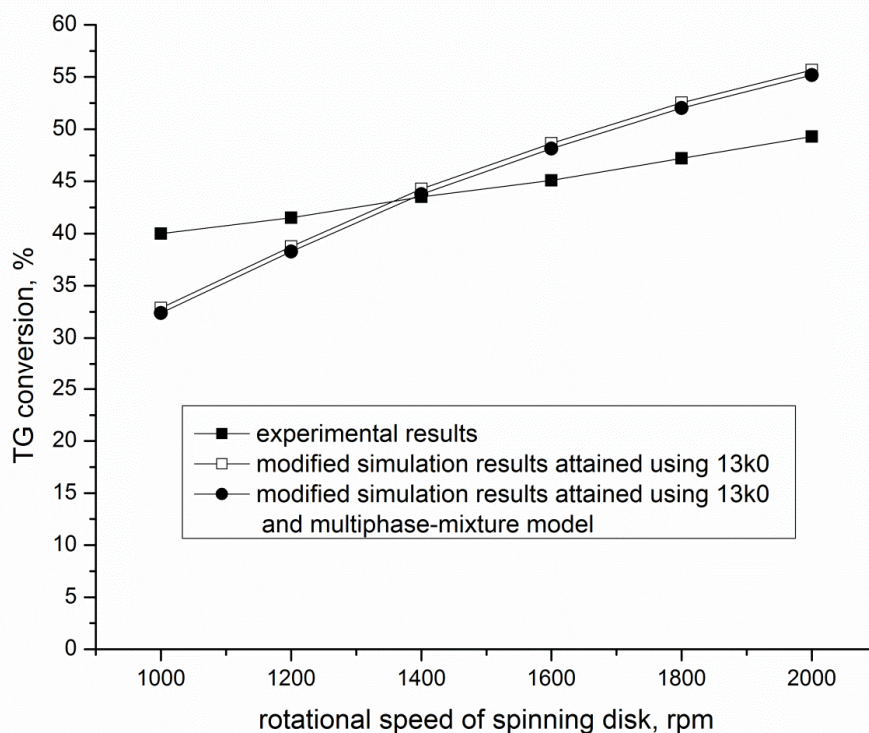


Fig. 12. Comparison of modified TG conversion attained by simulation using single phase model and using multiphase-mixture model.

From Fig. 12 we can see that simulated TG conversions obtained using the single phase model are slightly higher than those attained using of the multiphase model. This can be explained by the fact that mass transfer in the two-phase approach is always not as fast as in the single phase, in a well-mixed system. Slight differences between simulation results attained using the single phase model and those attained using the multiphase model indicate that flow in the SDR assumed to be single phase is satisfactory.

## 5. CONCLUSIONS

The CFD software ANSYS©Fluent v.13.0 was successfully used for a simulation of biodiesel synthesis from canola oil and methanol in the presence of a sodium hydroxide catalyst in the two-disc spinning disc reactor. To accomplish this task an adequate model of reaction with accompanying mass transfer was formulated and expressed in terms of facilities available within ANSYS©Fluent. This means that no advanced approach with a user defined function was necessary and thus we recommend the method for industrial applications when high accuracy is not required. The simulating results for several rotational speeds of the spinning disc were compared with corresponding experimental data obtained from a setup built at our collaborating partner from Kansas University. The modelling provided useful information about the reactor performance.

The hydrodynamics of reagents in the SDR provided insights into the fluid flow profiles in the inter-disc gap which could be helpful to explain how the fluid hydrodynamics influenced the performance of SDR. The reverse flow in the SDR helped to reach higher TG conversion, due to the increase of the residence time by expanding the zone of reverse flow in comparison to the “no-rotation” variant.

Due to the efficient mixing of reactants in SDR when the rotational speed of spinning disc is above 1000 rpm, single phase flow in SDR is assumed and is verified satisfactorily.

NaOH concentration highly influences kinetics and the kinetic rate constants are implicit functions of the catalyst concentration. In the present research, kinetic rate constants are obtained and modified on the basis of data from Nouredini and Zhu. When the content of TG in canola oil is 95%,  $13\{k_0\}$  was chosen as the kinetic constant data,  $\{k_0\}$  represents kinetic constant dataset used by Nouredini and Zhu.

The conversion achieved in the reactor was significantly influenced by the rotational speed of the upper disc. The faster the rotational speed of the upper disc is, the higher TG conversion can be achieved. Based on the experiment data of Zheyang Qiu and Weatherley, we can see that TG conversion obtained by simulation is acceptable. The discrepancy between the simulation and experiment results probably from the idealisation of the flow mechanism and the reaction model.

Our simulation results confirmed by the experiment indicated that above 1000 rpm rotational speed of spinning disc caused shorter residence time. This on the one hand helps to improve production efficiency and leads to less saponification and emulsification, consequently improves TG conversion. On the other hand, if the residence time is too short, it may be not sufficient for completing the reaction and consequently resulting in biodiesel yield decrease. One promising solution for the problem is a grooved disc design allowing for increase of the residence time, while still offering high mixing rates. This is planned for future investigation.

## SYMBOLS

$A_i$  pre-exponential factor,  $\text{m}^3\text{kmol}^{-1}\text{s}^{-1}$

$C_0$	TG molar concentration at inlet, $\text{kmol m}^{-3}$
$C_{j,r}$	molar concentration of species $j$ in reaction $r$ , $\text{kmol m}^{-3}$
$C_k$	TG molar concentration at outlet, $\text{kmol m}^{-3}$
$D$	diameter of the reactor, m
$d$	gap size of the reactor, m
$D_{i,m}$	mass diffusion coefficient for species $i$ in the mixture, $\text{m}^2\text{s}^{-1}$
$E_i$	activation energy, $\text{J kmol}^{-1}$
$H_i^0$	standard state enthalpy, $\text{J kmol}^{-1}$
$J_i$	diffusion flux of species $i$ , $\text{kmol m}^{-2}\text{s}^{-1}$
$k_{b,r}$	backward rate constant for the reaction $r$ , $\text{m}^3\text{kmol}^{-1}\text{s}^{-1}$
$k_{f,r}$	forward rate constant for the reaction $r$ , $\text{m}^3\text{kmol}^{-1}\text{s}^{-1}$
$k_i$	respective kinetic constant, $\text{m}^3\text{kmol}^{-1}\text{s}^{-1}$
$M_{w,i}$	the molecular weight of species $i$ , $\text{kg kmol}^{-1}$
$m$	number of cases simulated in the present research
$N$	spinning seed, rps
$N_R$	total number of reactions that species $i$ participate in
$n$	number of species
$P_{atm}$	atmospheric pressure (101325 Pa)
$Q_{v0}$	volume flow rate at inlet, $\text{m}^3\text{s}^{-1}$
$Q_{vk}$	volume flow rate at outlet, $\text{m}^3\text{s}^{-1}$
$R$	ideal gas constant, $\text{J kmol}^{-1}\text{K}^{-1}$
$R_i$	net rate of production of species $i$ by chemical reaction, $\text{kmol m}^{-3}\text{s}^{-1}$
$R'_{i,r}$	the Arrhenius molar rate of creation (or destruction) of species $i$ in reaction $r$ , $\text{kmol m}^{-3}\text{s}^{-1}$
$r_I, r_{II}, r_{III}$	reaction rate, $\text{kmol m}^{-3}\text{s}^{-1}$
$S_i$	rate of creation of species $i$ by additional source, $\text{kmol m}^{-3}\text{s}^{-1}$
$S_i^0$	standard state entropy, $\text{J kmol}^{-1}\text{K}^{-1}$
$T$	absolute temperature, K
$v_i$	velocity of species $i$ , $\text{ms}^{-1}$
$Y_i$	mass fraction of species $i$
<i>Greek symbols</i>	
$\kappa$	TG conversion
$\rho_i$	density of species $i$ , $\text{kg m}^{-3}$
$\mu$	viscosity, $\text{kg m}^{-1}\text{s}^{-1}$
$\vartheta'_{i,r}$	stoichiometric coefficient for reactant $i$ in reaction $r$
$\vartheta''_{i,r}$	stoichiometric coefficient for product $i$ in reaction $r$
$\eta'_{j,r}$	rate exponent for reactant species $j$ in reaction $r$
$\eta''_{j,r}$	rate exponent for product species $j$ in reaction $r$

## REFERENCES

- Brechtelsbauer C., Lewis N., Oxley P., Ricard F., Ramshaw C., 2001. Evaluation of a spinning disc reactor for continuous processing. *Org. Process Res. Dev.*, 5, 65-68. DOI: 10.1021/op0000834.
- Cafiero L.M., Baffi G., Chianese A., Jachuck R.J., 2002. Process intensification: precipitation of barium sulfate using a spinning disc reactor. *Ind. Eng. Chem. Res.*, 41, 5240-5246. DOI: 10.1021/ie010654w.
- Childs P.R.N., 2011. Rotating flow. *Elsevier Inc.*
- Cussler E.L., 1997. *Diffusion: Mass transfer in fluid systems*. 2nd edition, Cambridge University Press, New York, 111-120.
- Dehkordi A.M., 2002. Liquid-liquid extraction with chemical reaction in a novel impinging-jets reactor. *AIChE J.*, 48, 2230-2239. DOI: 10.1002/aic.690481013.

- Dehkordi A.M., Vafaieimanesh A., 2009. Synthesis of barium sulfate nanoparticles using a spinning disc reactor: Effects of supersaturation, disc rotation speed, free ion ratio, and disc diameter. *Ind. Eng. Chem. Res.*, 48, 7574-7580. DOI: 10.1021/ie801799v.
- Egbuna S.O., Ozonoh M., Aniokete T.C., 2013. Diffusion rate analysis in palm kernel oil extraction using different extraction solvents. *IJRET*, 02 (11), 639-648. DOI: 10.15623/ijret.2013.0211098.
- Freedman B., Butterfield R.O., Pryde E.H., 1986. Transesterification kinetics of soybean oil. *J. American Oil Chemists' Soc.*, 63, 1375-1380. DOI: 10.1007/BF02679606.
- Green A., Johnson B., John A., 1999. Process intensification magnifies profits. *Chem. Eng.*, 106, 66-73.
- Jachuck R., 2002. Process intensification for responsive processing. *TransIChemE*, 80, 233-238. DOI: 10.1205/026387602753581980.
- Krawczyk T., 1996. Biodiesel-alternative fuel makes inroads but hurdles remain. *INFORM*, 7, 801-82.
- Leveson P., Dunk W.A.E., Jachuck R.J., 2003. Numerical investigation of kinetics of free-radical polymerization on spinning disc reactor. *J. Appl. Polym. Sci.*, 90, 693-699. DOI: 10.1002/app.12762.
- Lodhar H., Jachuck R.J.J., 2007. Intensified biodiesel reaction using continuous rotating tube reactor technology. *Proceedings of the AIChE Annual Meeting*, Salt Lake City, USA.
- Meeuwse M., Hamming E., Schaaf J. van der, Schouten J.C., 2011. Effect of rotor–stator distance and rotor radius on the rate of gas–liquid mass transfer in a rotor–stator spinning disc reactor. *Chem. Eng. Process. Process Intensif.*, 50, 1095- 1107. DOI: 10.1016/j.cep.2011.05.022.
- Meeuwse M., Schaaf J. van der, Kuster B.F.M., Schouten J.C., 2010. Gas-liquid mass transfer in a rotor-stator spinning disc reactor. *Chem. Eng. Sci.*, 65, 466-471. DOI: 10.1016/j.ces.2009.06.006.
- Noureddini H., Zhu D., 1997. Kinetics of transesterification of soybean oil. *J. American Oil Chemists' Soc.*, 74, 1457-1463. DOI: 10.1007/s11746-997-0254-2.
- Przybylski R., 2007. Canola oil: Physical and chemical properties. Canola council of Canada web page.
- Qiu Z.Y., 2010. *Intensification of liquid-liquid contacting processes*. PhD Thesis, University of Kansas.
- Qiu Z.Y., Petera J., Weatherley L.R., 2012. Biodiesel synthesis in an intensified spinning disc reactor. *Chem. Eng. J.*, 210, 597-609. DOI: 10.1016/j.cej.2012.08.058.
- SAS IP, Inc., 2010. *ANSYS©Fluent v. 13.0 Theory Guide*.
- Stankiewicz A.I., Moulijn J.A., 2002. Process intensification: Transforming chemical engineering. *Chem. Eng. Prog.*, 96, 22-34.
- Tai C.Y., Tai C.T., Liu H.S., 2006. Synthesis of submicron barium carbonate using a high-gravity technique. *Chem. Eng. Sci.*, 61, 7479-7486. DOI: 10.1016/j.ces.2006.08.065.
- Tai C.Y., Tai C.T., Chang M.H., Liu H.S., 2007. Synthesis of magnesium hydroxide and oxide nanoparticles using a spinning disc reactor. *Ind. Eng. Chem. Res.*, 46, 5536-5541. DOI: 10.1021/ie060869b.
- Tai C.Y., Wang Y.H., Tai C.T., Liu H.S., 2009. Preparation of silver nanoparticles using a spinning disc reactor in a continuous mode. *Ind. Eng. Chem. Res.*, 48, 10104-10109. DOI: 10.1021/ie9005645.
- Van Eeten K.M.P., Van der Schaaf J., Schouten J.C. and Van Heijst G.J.F., 2012. Boundary layer development in the flow field between a rotating and a stationary disc. *Phys. Fluids*, 24, 033601. DOI: 10.1063/1.3698406.
- Visscher F., Hullu J., Croon M.H.J.M., Schaaf J., Schouten J., 2013. Residence time distribution in a single-phase rotor-stator spinning disc reactor. *AIChE J.*, 59, 2686–2693. DOI: 10.1002/aic.14036.

Received 05 May 2014

Received in revised form 22 December 2014

Accepted 10 January 2015

## APPENDIX

Explicit rate equations for each individual component, TG, DG, MG, GL, CH<sub>3</sub>OH and biodiesel are as follows.

For reaction I:

$$R'_{TG,I} = R'_{CH_3OH,I} = -(k_1[C_{TG}][C_{CH_3OH}] - k_2[C_{DG}][C_{biodiesel}]) \quad (A-1)$$

$$R'_{DG,I} = R'_{biodiesel,I} = k_1[C_{TG}][C_{CH_3OH}] - k_2[C_{DG}][C_{biodiesel}] \quad (A-2)$$

For reaction II:

$$R'_{DG,II} = R'_{CH_3OH,II} = - (k_3[C_{DG}][C_{CH_3OH}] - k_4[C_{MG}][C_{biodiesel}]) \quad (A-3)$$

$$R'_{MG,II} = R'_{biodiesel,II} = k_3[C_{DG}][C_{CH_3OH}] - k_4[C_{MG}][C_{biodiesel}] \quad (A-4)$$

For reaction III:

$$R'_{MG,III} = R'_{CH_3OH,III} = - (k_5[C_{MG}][C_{CH_3OH}] - k_6[C_{GL}][C_{biodiesel}]) \quad (A-5)$$

$$R'_{GL,III} = R'_{biodiesel,III} = k_5[C_{MG}][C_{CH_3OH}] - k_6[C_{GL}][C_{biodiesel}] \quad (A-6)$$

Thus,

$$R'_{TG} = R'_{TG,I} = - (k_1[C_{TG}][C_{CH_3OH}] - k_2[C_{DG}][C_{biodiesel}]) \quad (A-7)$$

$$\begin{aligned} R'_{DG} &= R'_{DG,I} + R'_{DG,II} = \\ &= k_1[C_{TG}][C_{CH_3OH}] - k_2[C_{DG}][C_{biodiesel}] - (k_3[C_{DG}][C_{CH_3OH}] - k_4[C_{MG}][C_{biodiesel}]) \end{aligned} \quad (A-8)$$

$$\begin{aligned} R'_{MG} &= R'_{MG,II} + R'_{MG,III} = \\ &= k_3[C_{DG}][C_{CH_3OH}] - k_4[C_{MG}][C_{biodiesel}] - (k_5[C_{MG}][C_{CH_3OH}] - k_6[C_{GL}][C_{biodiesel}]) \end{aligned} \quad (A-9)$$

$$R'_{GL} = R'_{GL,III} = k_5[C_{MG}][C_{CH_3OH}] - k_6[C_{GL}][C_{biodiesel}] \quad (A-10)$$

$$\begin{aligned} R'_{CH_3OH} &= R'_{CH_3OH,I} + R'_{CH_3OH,II} + R'_{CH_3OH,III} = \\ &= - (k_1[C_{TG}][C_{CH_3OH}] - k_2[C_{DG}][C_{biodiesel}]) - (k_3[C_{DG}][C_{CH_3OH}] - k_4[C_{MG}][C_{biodiesel}]) + \\ &\quad - (k_5[C_{MG}][C_{CH_3OH}] - k_6[C_{GL}][C_{biodiesel}]) \end{aligned} \quad (A-11)$$

$$\begin{aligned} R'_{biodiesel} &= R'_{biodiesel,I} + R'_{biodiesel,II} + R'_{biodiesel,III} = \\ &= k_1[C_{TG}][C_{CH_3OH}] - k_2[C_{DG}][C_{biodiesel}] + k_3[C_{DG}][C_{CH_3OH}] - k_4[C_{MG}][C_{biodiesel}] + \\ &\quad + k_5[C_{MG}][C_{CH_3OH}] - k_6[C_{GL}][C_{biodiesel}] \end{aligned} \quad (A-12)$$